TO MEASURE CRACKS IN REINFORCED CONCRETE BEAM WITHOUT PRIOR DETECTION, APPLICATION TO DIFFUSE CRACKING EVALUATION

GUILLAUME EWALD[*] AND YANN MALECOT[†]

[*] Univ. Grenoble Alpes, CNRS, Grenoble INP, 3SR, Grenoble, 38000, France
e-mail: guillaume.ewald@univ-grenoble-alpes.fr

[†] Univ. Grenoble Alpes, CNRS, Grenoble INP, 3SR, Grenoble, 38000, France

Key words: DIC, crack kinematics, lagrangian displacement gradient, diffuse cracking, stereology

Abstract. In recent years, local Digital Image Correlation has become a standard method to monitor cracks in concrete samples during laboratory tests, aiding the understanding of fracture mechanisms. The significant challenge is to efficiently and accurately evaluate crack characteristics from the DIC displacement field. Most existing methods, when they do not employ machine learning techniques in the middle, start with crack extraction. This is usually based on DIC residuals, strain analysis or image processing. The discontinuity kinematic can then be evaluated using points on both sides of the crack and usually require prior crack local frame computation in addition.

This paper applies a streamlined method for crack measurement to four-point bending tests on RC beams. The method bypasses the need for crack geometry extraction, local frame calculation and point selection, directly analyzing the full displacement gradient field. Taking advantage of the rather simple displacement field around cracks, the local crack kinematics—such as opening, slip, and orientation—are continuously calculated at all displacement points. The opening and slip measures are maximal along cracks, allowing easy crack extraction after crack kinematic evaluation.

RC beams with varying shear reinforcement ratios are studied, demonstrating the method's capability to analyze complex crack patterns. Furthermore, this procedure can be easily adapted for 3D Digital Volume Correlation (DVC) displacement fields obtained from microtomography with minimal modification, offering broader applicability to both experimental and numerical displacement fields, an advantage over conventional methods.

1 Introduction

Concrete is a brittle material. Experimental structural concrete research is often based on crack evaluation (position, kinematic, evolution), whether to understand the mechanisms of ruin and assess model performance or to characterise the behaviour of cement based composites or new manufacturing processes.

For this propose local Digital Image Correlation (DIC) has been widely used in the past few years, since it provides the full displacement field on the observed concrete member surface. To extract the crack kinematics from the displacement field, The Automated Crack Detection Method (ACDM) [1, 2] has established itself as the reference method proposing to automatically compute crack kinematics with points selected on both sides of the pre-detected crack.

The author will submit shortly an alternative method for crack measurement, the Crack Is Montain (CIM) method, that does not require determining the position of the crack tak-

ing advantage of the simplification crack induces on the Lagrangian displacement gradient [3]. The result is a crack kinematic field that is null where there is no crack and equal to the displacement discontinuity intensity at cracks. They validated the method confronting it with the results provided by ACDM on the critical shear crack of an RC beam under 4 points bending.

This paper applies the CIM method to 4 beams subjected to 4 points bending but this time the analysis is not limited to the single critical shear crack. The full patterns is investigated to illustrate the kind of information the method can lead to. In particular, given the shape of the kinematic field, stereological technics [4] appear to be adapted to provide a statistic of the crack distribution.

2 Crack Is Mountain (CIM), a crack measurement method

The input of the CIM is a point-based displacement field like DIC can return. Due to the cracks the displacement full field exhibits discontinuities. They are to be analysed to recover the crack kinematic.

To directly compute the crack kinematic without previous crack detection the CIM proposes to analyze the lagrangian displacement gradient. Hence, it needs a robust and reliable gradient calculation.

Then the kinematic computation makes use of the kinematics' implications of cracking to extract the displacement discontinuity from the gradient around the crack. The method is straightforward but requires extra care to manage non-local rotations.

For the full demonstration, the interested reader is referred to the master paper [3]. Only the useful formulae are recalled here.

2.1 Lagrangian displacement gradient calculation by linear local regression

A local linear regression [5] is implemented to compute the Lagrangian displacement gradient. Given a neighbourhood $\mathcal{V}(\alpha)$ of the calculation point α, the contribution of a neighbour

point β in $\mathcal{V}(\alpha)$ is weighted using a weighting function $w_{l_g}(r)$ of the distance r between points α and β, expressed pixel (px). In the following, the weighting function is Gaussian; a characteristic length l_g is introduced:

$$w_{l_g}(r) = \begin{cases} \exp\left(-\frac{1}{2}\left(\frac{r-1}{l_g/3}\right)^2\right) & \text{if } r \in [1, l_g + 1] \\ 0 & \text{else} \end{cases} \tag{1}$$

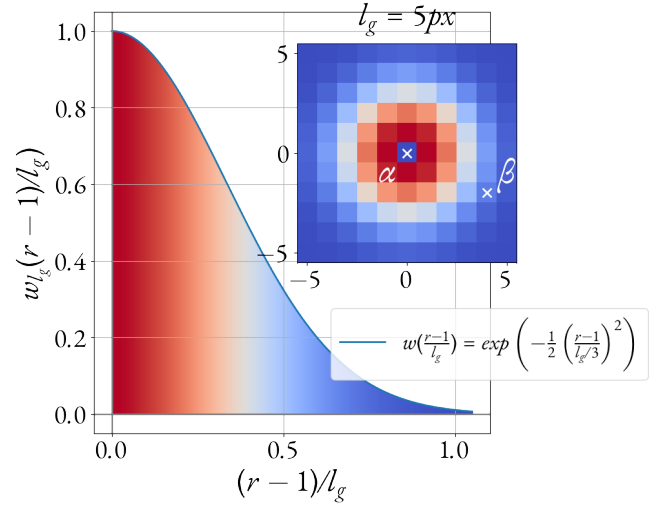The neighborhood definition is illustrated (*fig.*1)

Figure 1: Weighting function: graph and surface representation

Noting, $\underline{X}^{\alpha\beta} = \underline{X}^{\beta} - \underline{X}^{\alpha}$ the vector from $\underline{X}^{\alpha}$ to $\underline{X}^{\beta}$, respectively α and β positions, $\underline{u}^{\alpha\beta} = \underline{u}(\underline{X}^{\beta}) - \underline{u}(\underline{X}^{\alpha})$, the displacement difference between points α and β, and

$$\underline{\underline{\omega}}^{\alpha} = \sum_{\beta \in \mathcal{V}(\alpha)} w_{l_g}(||\underline{X}^{\alpha\beta}||)\, \underline{u}^{\alpha\beta} \otimes \underline{X}^{\alpha\beta} \tag{2}$$

$$\underline{\underline{\eta}}^{\alpha} = \sum_{\beta \in \mathcal{V}(\alpha)} w_{l_g}(||\underline{X}^{\alpha\beta}||)\, \underline{X}^{\alpha\beta} \otimes \underline{X}^{\alpha\beta} \tag{3}$$

the Lagrangian displacement gradient is expressed,

$$\underline{\underline{A}}^{\alpha} = \underline{\underline{\omega}}^{\alpha} \cdot \left(\underline{\underline{\eta}}^{\alpha}\right)^{-1} \tag{4}$$

The only parameter to compute the displacement gradient is the length l_g, parameter of the weighting function. It is the only parameter for the evaluation of the crack kinematics presented in the next section.

2.2 Crack measurement from displacement gradient

The displacement field is supposed to be locally constant by part through cracks. The displacement discontinuity in a crack local frame $(\underline{l}, \underline{n})$, $\underline{l}$ being the vector tangent to the crack and $\underline{n}$ normal as shown is (*fig*.2), is expressed,

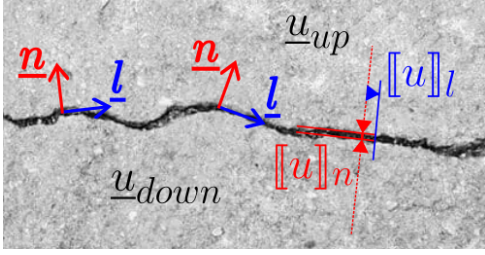$$[\![\underline{u}]\!] = [\![u]\!]_l \, \underline{l} + [\![u]\!]_n \, \underline{n} \qquad (5)$$

Figure 2: Crack local frame and kinematic

In the following, the crack orientation, defined as the angle between $\mathbf{t}_l$ and the horizontal direction, will be denoted as θ. The discontinuity direction angle, representing the angle between the displacement discontinuity vector $[\![\mathbf{u}]\!]$ and the horizontal, will be denoted as β.

Taking into account a small non-local rotation of angle α this implies the displacement gradient in the local frame to be,

$$\underline{\underline{A}} = \begin{pmatrix} 0 & A_{l_g}([\![u]\!]_l) + \alpha \\ -\alpha & A_{l_g}([\![u]\!]_n) \end{pmatrix}_{(\underline{l},\underline{n})} \qquad (6)$$

with A_{l_g} a linear function that links the displacement discontinuity components to the displacement gradient. $A_{l_g}([\![u]\!]_n)$ can be directly computed from the gradient in the local frame using the trace,

$$A_{l_g}([\![u]\!]_n) = \operatorname{tr} \underline{\underline{A}} \qquad (7)$$

and $A_{l_g}([\![u]\!]_n)$ considering the invariant of the symmetric part of the gradient,

$$A_{l_g}([\![u]\!]_l)^2 = (A_{12} + A_{21})^2 - 4A_{11}A_{22} \qquad (8)$$

The function A_{l_g} can be computed analytically or numerically. In the case of a perfectly sharp crack,

$$\frac{A_{l_g}([\![u]\!])}{[\![u]\!]} = \frac{2}{\pi} \frac{\int_{Supp(w_{l_g})} r^2 w_{l_g}(r) \, dr}{\int_{Supp(w_{l_g})} r^3 w_{l_g}(r) \, dr} \qquad (9)$$

To define the crack local frame the rotation has to be computed,

$$2\alpha = A_{12} - A_{21} - sign\left(\det \underline{\underline{A}} \times (A_{12} - A_{21})\right) \\ \times (a_{12} - a_{21}) + O(\alpha^2) \qquad (10)$$

$(\underline{\underline{A}} - \underline{\underline{R}}(\alpha))^T \cdot (\underline{\underline{A}} - \underline{\underline{R}}(\alpha))$ has only one non-null eigenvalue associated to $\underline{n}$, $\underline{l}$ being the other eigenvector.

The displacement gradient is defined at every point. So are the crack measures.

3 Experimental program

It is proposed as an application to compare crack patterns of RC beams with different transverse reinforcement ratios and geometries using the CIM. The comparison is not extensive and just aims to illustrate statistics that can be computed with the method.

3.1 Test specimens

Four beams with four transverse reinforcement configurations as part of a wider experimental campaign [6] were tested. The geometry of the beams remains the same, square sections with sides of $300 \ mm$ and with a total length of $2300 \ mm$. The distance between the supports is $2000 \ mm$ and between the load application points $600 \ mm$ leaving two $700 \ mm$. The beams are speckled to perform DIC afterwards. The experimental setup is illustrated (*fig*.3). The selected beams are referred to as K2, L1, M1 and N1 in the aforementioned study [6].
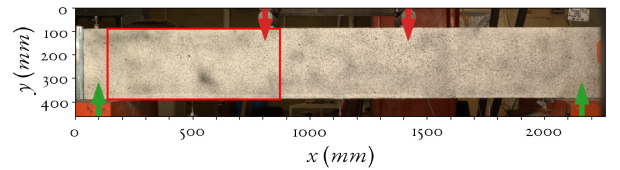

Figure 3: Experimental setup, speckled beam, left shear midspan framed, load application points in red, support in green

3

The beams present a great amount of longitudinal reinforcement, $6 \times \phi 25mm$ rebar, to enforce shear failure. Concerning the transverse reinforcement different rebar diameters, ϕ, spacing, s, inclination, i, are tested, see (*tab.*4).

$\phi\,(mm)$	$s\,(mm)$	$i\,(°)$	$\rho\,(mm^2/mm^2)$	ID
8	70	90	4.8×10^{-3}	$\phi 8s70i90$
8	210	45	1.6×10^{-3}	$\phi 8s210i45$
8	210	90	1.6×10^{-3}	$\phi 8s210i90$
14	210	90	4.9×10^{-3}	$\phi 14s210i90$

Figure 4: Test specimens parameters

3.2 4 points bending load-deflection curves

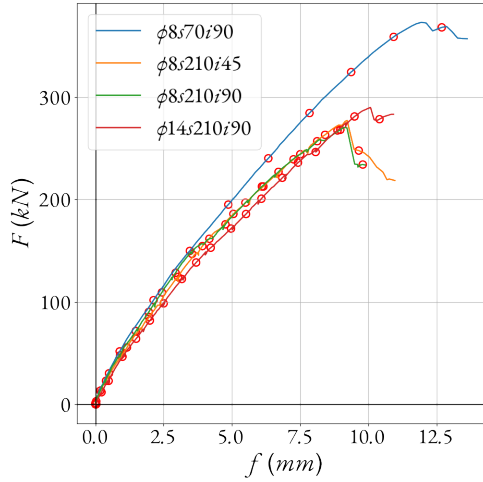The load-deflection curve, $F(f)$, of each specimen is presented (*fig.*5).

Figure 5: Load (F) Deflection (f) curves and selected loadstep used for evolution analysis

It appears that beams $\phi 8s210i90$ and $\phi 8s210i45$ exhibit the same behaviour, the first being slightly stiffer at the beginning before shear cracks propagate. Despite beams $\phi 8s70i90$ and $\phi 14s210i90$ having approximately the same reinforcement ratio, the response of the latter is closer to the response of $\phi 8s210i90$ that has a reinforcement ratio 3 times smaller with only a slight improvement of the shear bearing capacity.

Roughly speaking, the structural behaviour seems dictated by the transverse displacement spacing more than by the shear reinforcement ratio and the shear reinforcement inclination.

3.3 Displacement calculation by DIC

Digital image correlation (DIC) was performed using the PYTHON library SPAM [7]. The region of interest measures $2700\,px$ in length and $1100\,px$ in width with a pixel size of $3/11\,mm$. The correlation was conducted with round subsets of diameter $ws = 20\,px$ arranged on a regular grid, with points spaced every $st = 4\,px$.

The correlation is performed at each time step by comparing the current image to a reference image taken before loading. The algorithm uses the sum of the last computed displacement and the last displacement increment as the initial guess for the subsequent step.

The interpolation of the subset grey levels is conducted using first-order polynomials and only rigid motion of the subsets are looked into.

The CIM is applied with a internal gradient internal length $l_g = 40\,px$.

3.4 Noise level

The two first images serve respectively as reference for the DIC and for noise evaluation. Here only the crack opening noise computed with the two first images for each sample is presented (*fig.*6) to define a minimal measurable crack kinematics.
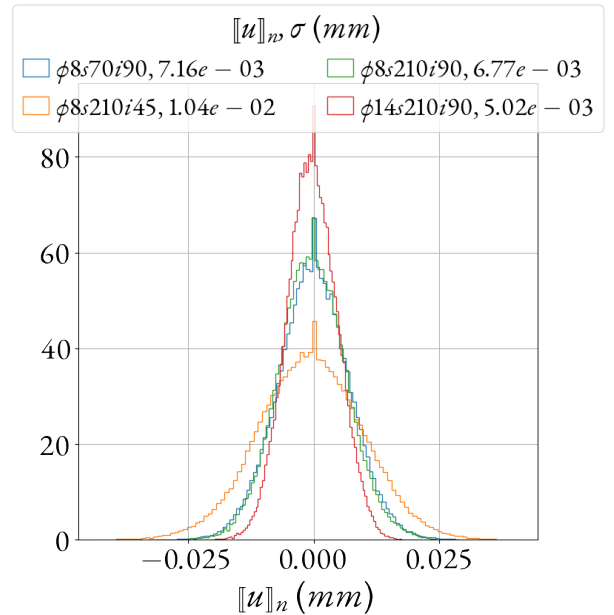

Figure 6: opening noise

Depending on the light and the speckle the noise is not the same for all beams. $0.035\,mm$ is taken as the minimal measurable crack opening, which will serve in the following.

3.5 CIM crack measure

The crack kinematic returned by the the CIM method is defined on the whole surface but is only meaningfull at crack where the crack displacement is not null. The best plot to illustrate the measure is a 3D surface provided (*fig.*7).
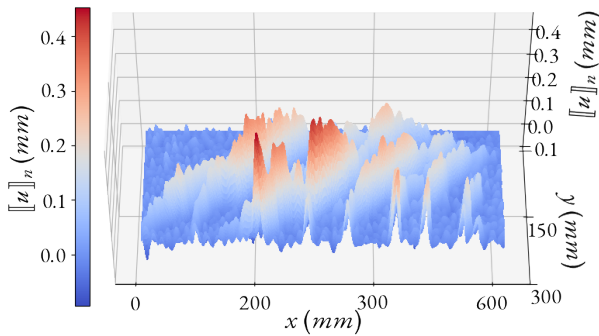

Figure 7: $\phi8s70i90$, Crack opening fields, prior shear failure, $f = 9.4\,mm$

The crack measure are the intensities of the ridges of the field.

4 Crack pattern analysis

After computing all displacement fields, the CIM applied, and the noise evaluated, it is proposed to analyse the crack pattern to explain the beams behaviour before the first shear failure.

4.1 Crack kinematics

The CIM method returns crack kinematics fields on the complete observed surface. Such fields for the four beams just before the shear failure are represented (*fig.*8).
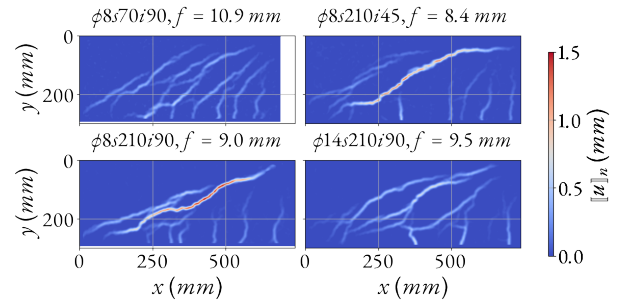

Figure 8: Crack opening fields, prior beams failure, prior shear failure

The resulting fields resemble those obtained from strain measurements; however, along cracks, the intensity represents crack kinematics, as the strain itself lacks physical significance in these regions.

In this study, the four tested beams exhibit different crack patterns, seemingly influenced by the transverse reinforcement spacing. The three beams with a transverse reinforcement spacing of 210 mm develop more widely spaced cracks compared to the beam with 70 mm spacing, where cracks are distributed more uniformly across the midspan. A common feature among all specimens is the horizontal propagation of shear cracks at both ends of the beam. At the bottom, this propagation appears to result from the heavy longitudinal reinforcement, which tends to promote the Goujon effect.

Crack opening also seems to depend on the reinforcement ratio. Beams $\phi8s70i90$ and $\phi14s210i90$ exhibit a maximum crack opening of approximately 0.6 mm, while beams $\phi8s210i90$ and $\phi8s210i45$ reach around 1.2 mm. Additionally, crack opening in the first two beams is more evenly distributed among multiple cracks, whereas in the latter two, it is concentrated in fewer cracks, favoring the development of larger individual openings.

The crack opening field provides both qualitative insights into the crack pattern and quantitative information on crack kinematics, usefull for many crack-based studies in structural concrete analysis.

4.2 Crack orientation and displacement discontinuity direction

The local basis provided by the CIM defines the crack orientation angle, denoted θ, along with the kinematic components in the local coordinate system: crack opening and slip. The direction of the displacement discontinuity is noted as β. Although these quantities are computed throughout the entire domain, they are meaningful only at crack locations. To analyze the directional properties of the crack pattern, a threshold is applied based on the noise level computed in Section 3.4. The orientation histograms exhibit two distinct peaks: one corresponding to flexural cracks and the other to shear cracks. To determine the preferred directions, a double Gaussian function is fitted to the data to separate the two crack types, as illustrated in Figure 9.
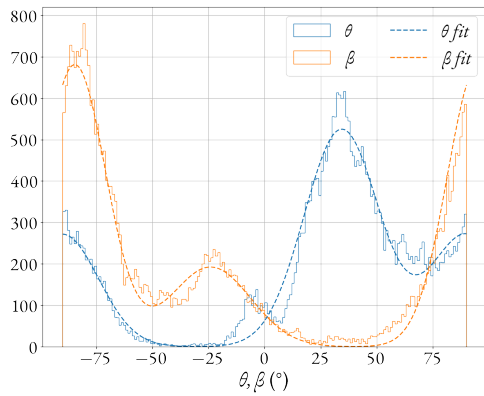

Figure 10: Crack and discontinuity orientations

Figure 9: Crack orientation (θ) and displacement discontinuity direction (β) and double gaussian fit prior failure; shear cracks are predominant

	$\phi 8s70i90$	$\phi 8s210i45$	$\phi 8s210i90$	$\phi 14s210i90$
θ (°)	47	34	35	37
β (°)	-81	-84	-83	-86

Figure 11: shear cracks : mean values of inclination of cracks and orientation of displacement discontinuity

Fitting the crack inclination distribution with a bell curve is a significant simplification, as crack orientation is not a random process but rather influenced by the stress state and geometry of reinforcements. Notably, shear cracks often exhibit a curved shape.

Each distribution reveals two peaks associated with flexural and shear cracks, where flexural cracks have an orientation around $\pm 90°$ and a discontinuity vector close to $0°$. Furthermore, the angle between the crack orientation θ and the opening direction β exceeds $90°$, indicating that crack slip arises not only from crack tortuosity but also from the test geometry.

The difference between θ and β consistently exceeds $90°$; systematic crack slip occurs, the latter cannot be attributed solely to crack roughness.

The orientation histograms for all beams just prior to shear failure are presented in Figure 10. The preferred crack orientations are summarized in Table 11.
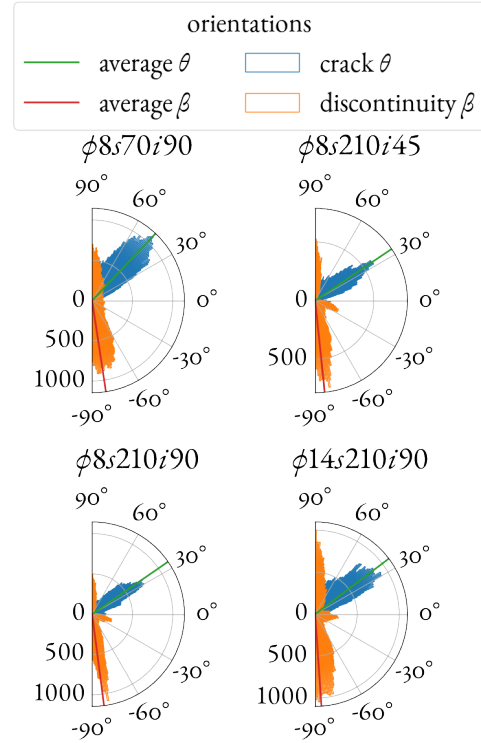
4.3 Stereology and Crack statistics

A key counterintuitive aspect of the CIM is that the crack information is continuous across the entire surface, whereas cracks are, by definition, discrete. One way to compute crack statistics is to adopt a stereological approach that is based on counting events on lines.

Grid oriented with several angle $\theta_{grid} \in [0, 180°]$ are superimposed with the cracked surface like the $\theta_{grid} = 135°$ case illustrated in (*fig.*12). for all orientations and is set to 80 px in this study.
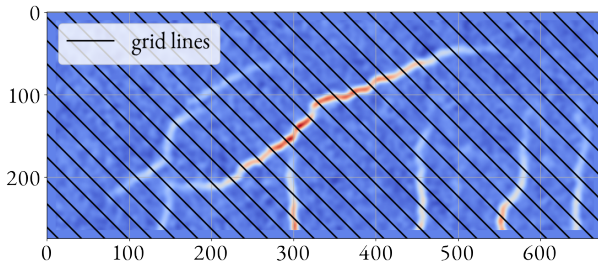

Figure 12: Counting grid $\theta_{grid} = 135°$, distance between lines $80\,px = 22\,mm$, prior shear failure

Simple tools, like peaks detection, allow to count the number of intersections between the grid lines and the crack for several θ such as the probability of the grid intersecting a crack can be estimated. This latter quantity is linked to the total crack length by the formula [4, 8],

$$\frac{L_{crack}^{tot}}{S_{beam}} = \frac{\pi}{2}\frac{\overline{N_{intersec}}}{L_{grid}} \tag{11}$$

with $N_{intersec}$ the intersection count and L_{grid} the total grid length, the $\frac{\overline{N_{intersec}}}{L_{grid}}$ meaning the mean on all the directions. The first column in (*fig.*13) shows the count as a function of the angle for the 4 beams.

Similarly, the sum of the crack openings at the intersection points between the grids and the cracks can be computed to provide information on the orientation of the actively opening cracks. Peak detection must account for the opening noise, set to 0.035 mm, ensuring that the total measured crack length corresponds to cracks with openings exceeding this threshold.

The intersection and opening count rose diagrams are presented in the second column of Figure 13.
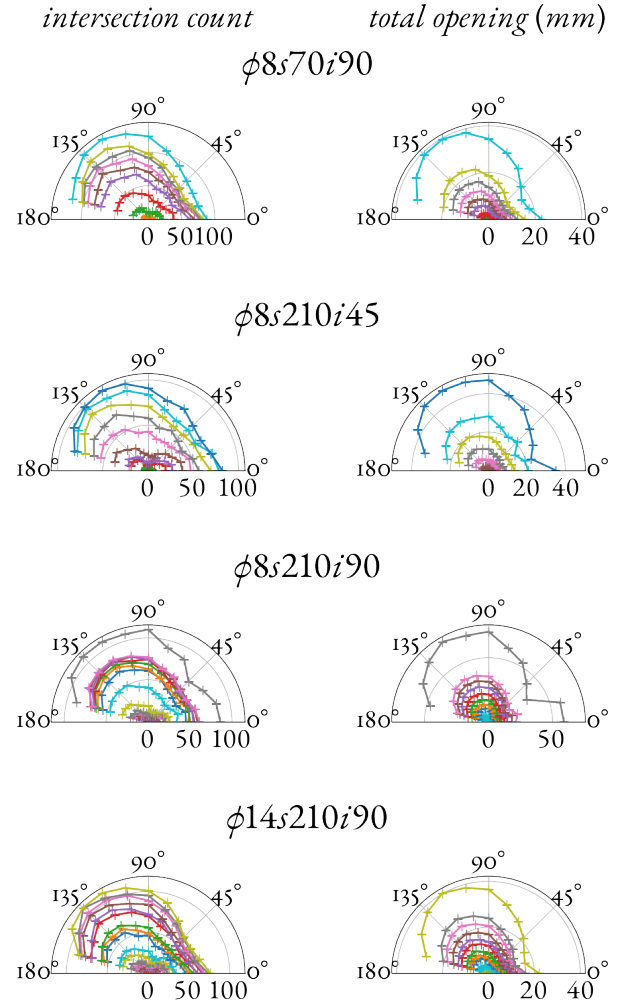

Figure 13: Intersection count with $0.035\,mm$ threshold and total opening of cracks versus θ_{grid} for the selected loadstep in (*fig.*5)

Except for $\phi 8s210i90$, (*fig.*13) show that the failure is not associated with a crack propagation but with sudden opening of the shear crack that are count for $\theta_{grid} \approx 135°$ given (*fig.*12). The

Finally, Figure 14 presents the total crack length, the maximum crack opening and the standard deviation of the crack opening peaks at peaks on the grid. As previously mentioned, the crack opening is influenced by the reinforcement ratio. Beam failure appears to occur in

two distinct phases: the first phase is marked by crack propagation with limited maximum crack opening and without to much disparity between cracks, while the second involves significant crack opening with restricted crack propagation. This second phase coincides with the formation of a single dominant crack rather than multiple cracks, as qualitatively observed, and is delayed in beams with higher reinforcement ratios.
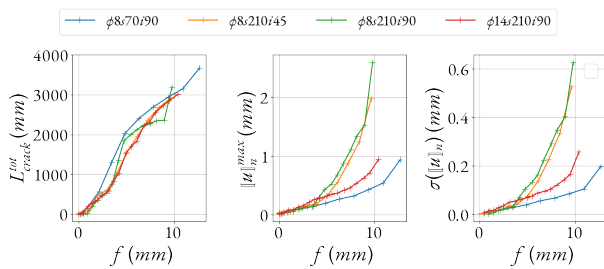

Figure 14: Total crack length with opening greater than 0.035 mm, max crack opening and standard deviation of opening on intersection

5 Conclusion

The CIM method enables to measure crack from DIC displacement fields without prior localisation. The kinematic results are defined all over the correlated surface and meaningfull where the discontinuity measure is not null.

The fields themselves are very usefull to monitor crack opening, the crack lips relative displacement and orientation. For further analysis, a stereological approach can be effectively performed to get more quantitative informations on the crack pattern such as crack total length or crack distribution.

Another advantage of this method lies in its adaptability to 3D analysis using DVC displacement fields, where crack surface extraction can be particularly challenging. This aspect will be the focus of the authors' future work.

REFERENCES

[1] N. Gehri, J. Mata-Falcón, and W. Kaufmann. Automated crack detection and measurement based on digital image correlation. Construction and Building Materials, 256:119383, September 2020.

[2] N. Gehri, J. Mata-Falcón, and W. Kaufmann. Refined extraction of crack characteristics in large-scale concrete experiments based on digital image correlation. Engineering Structures, 251:113486, January 2022.

[3] G. Ewald and Y. Malecot. Lagrangian displacement gradient-based crack measurement, application to DIC displacement field. under submission.

[4] H. Solomon. Geometric Probability. CBMS-NSF Regional Conference Series in Applied Mathematics. Society for Industrial and Applied Mathematics, January 1978.

[5] M. G. D. Geers, R. De Borst, and W. A. M. Brekelmans. Computing strain fields from discrete displacement fields in 2D-solids. International Journal of Solids and Structures, 33(29):4293–4307, December 1996.

[6] Doraine Rouphael, Florent Vieux-Champagne, Yannick Sieffert, and Yann Malecot. Shear behavior of reinforced concrete beams with wire rope shear reinforcement. Materials and Structures, 56(6):114, July 2023.

[7] O. Stamati, E. Andò, and E. Roubin et al. 'spam': Software for Practical Analysis of Materials. Journal of Open Source Software, 5(51):2286, July 2020.

[8] R. R. A. Morton. The Expected Number and Angle of Intersections between Random Curves in a Plane. Journal of Applied Probability, 3(2):559–562, 1966. Publisher: Applied Probability Trust.